PCCP
Physical Chemistry Chemical Physics

Accepted Manuscript

This article can be cited before page numbers have been issued, to do this please use: Y. Fu, S. Xiao, S. Liu, J. Wu, X. Wang, L. Qiao, Z. Zhang and J. He, *Phys. Chem. Chem. Phys.*, 2020, DOI: 10.1039/D0CP03092A.

ROYAL SOCIETY OF CHEMISTRY

rsc.li/pccp

Stability, deformation and rupture of Janus oligomer enabled self-emulsifying water-in-oil microemulsion droplet

Yuequn Fu,[a] Senbo Xiao,[*a] Siqi Liu,[a] Jianyang Wu,[b] Xiao Wang,[c] Lijie Qiao,[d] Zhiliang Zhang[a] and Jianying He[* † a, d]

[a]NTNU Nanomechanical Lab, Norwegian University of Science and Technology (NTNU), Trondheim 7491, Norway

[b]Department of Physics, Research Institute for Biomimetics and Soft Matter, Jiujiang Research Institute and Fujian Provincial Key Laboratory for Soft Functional Materials Research, Xiamen University, Xiamen 361005, China

[c]Reservoir Engineering Research Institute, Palo Alto, California 94301, United States

[d]Beijing Advanced Innovation Center for Materials Genome Engineering, University of Science and Technology Beijing, Beijing 100083, China

[*]Corresponding author.
E-mail addresses: senbo.xiao@ntnu.no (S. Xiao), jianying.he@ntnu.no (J. He).

[†]Currently on sabbatical as a visiting professor at [d]Beijing Advanced Innovation Center for Materials Genome Engineering, University of Science and Technology Beijing.

Abstract

Microemulsion exists widely in nature, daily life and industrial manufacturing, including petroleum production, food processing, drug delivery, new materials fabrication, sewage treatment, etc. The mechanical properties of microemulsion droplets and the correlation to their molecular structures are of vital importance to those applications. Despite researches on their physicochemical determinants, there are lots of challenges to explore the mechanical properties of microemulsion by experimental studies. Herein, atomistic modelling was utilized to study the stability, deformation, and rupture of Janus oligomer enabled water-in-oil microemulsion droplets, aiming for revealing their intrinsic relationship to the Janus oligomer based surfactants and oil structures. The self-emulsifying process from a water, oil and surfactant mixture to a single microemulsion droplet was modulated by the amphiphilicity and the structure of the surfactants. Four microemulsion systems with interfacial thickness in the range of 7.4-17.3Å were self-assembled to explore the effect of the surfactant on the droplet

morphology. By applying counter forces on the water core and the surfactant shell, the mechanical stability of microemulsion droplets was probed at different ambient temperatures. A strengthening response and a softening regime before and after a temperature-dependent peak force were identified followed by the final rupture. This work demonstrates a practical strategy to precisely tune the mechanical properties of a single microemulsion droplet, which can be applied in the formation, de-emulsification, and design of microemulsion in oil recovery and production, drug delivery and many other applications.

Key Words: Self-emulsifying; microemulsion droplet; stability; deformation; rupture; molecular dynamics simulation.

1 INTRODUCTION

The microemulsion is thermodynamic-stable mixtures of multiphase system, and in many cases presents as droplets of one liquid dispersed inside the other surrounding liquid[1-3]. Because microemulsion plays an important role in daily life and applications including wastewater treatment[4, 5], drug-delivery[6], electro-kinetic chromatography[7, 8], enhanced oil recovery[9], fabrication of new materials[10], nanoparticle synthesis[11], and many others, it has been the focus of many research fields for decades.

Research on microemulsions started in 1943 when microemulsion as a scientific concept was first promoted by Hoar and Schulman[12]. With limited experimental characterization methods, spontaneous formation of globular micelles with size ~120 Å in diameter was identified, which clearly explained how the orientated non-ionized amphipathic molecules prevented the ion-pairs of soap from the repulsion. In 1959 microemulsion was characterized by electron microscopy and demonstrated a uniformly dispersed spherical oil or water core in water or oil droplet[13]. The detailed structural and dynamic properties of the chemical ingredients of microemulsion were then investigated by Fourier transform nuclear magnetic resonance (FT-NMR), which provided a clear picture of the polydisperse nature of the complex multiphase system[14-16]. Other experimental methodologies, such as infrared and Raman spectroscopy, were also applied in studying microemulsion to gain a better understanding of nanoscale morphologies[17, 18]. It is generally accepted nowadays in the nanotechnology era that microemulsion is a colloid system consisting of small droplets of water (or oil), which could be on the nanometer scale, dispersed in a continuum medium of oil (or water) phase by adding surfactant and/or cosurfactant as stabilizer. The highly complicated nature of the surfactant

layer on microemulsion droplets is currently attracting attention from different research fields, and continually provides new multi-disciplinary insights[19, 20].

The most important property of the microemulsion is its thermodynamic stability[21, 22]. The surfactant and cosurfactant coating on the surface of the emulsion droplets greatly reduces the interfacial tension between the continuum phase and the interior of the droplet, minimizing the overall free energy of the microemulsion system[23]. There are many factors affecting the stability of a microemulsion system, including temperature, salinity, surfactant structure, oil composition, cosolvent, and immiscible solids, and their effects are inherently intertwined[24, 25]. It is highly challenging in experiments to clarify the intricate relationship between each factor and the stability of the microemulsion system. In contrast, atomistic modeling and molecular dynamic (MD) simulations can provide resolution extending the experimental limits in investigating microemulsion. For instance, a series of MD simulations were performed to probe the properties of water/trichloroethylene (TCE) interface absorbed with sodium alkyl sulfate (SDS-type) surfactant monolayers, and further to elucidate the underlying connections between the parameters of a microemulsion system. The results revealed that the tail order of the surfactants was dependent on their interfacial coverage, while the interface thickness (in the range of 10-25 Å) was interestingly dependent on tail length rather than the surface coverage[26].

Comparing to the fast accumulation of synthesis and physicochemical knowledge on microemulsion, the mechanical stability of microemulsion still awaits a thorough investigation. The mechanical stability of microemulsion is crucially important in many production and application processes[27-29]. For instance, microemulsion was utilized in drug delivery, where the mechanical robustness of the microemulsion droplets are critical to the transport and the release of the loaded drug[30]. The nanomechanics of microemulsion droplets is the determinant of the de-emulsification process on oil/water separation in oil production, which prominently influences the production cost in the petroleum industry[31]. However, there are still lots of challenges for experimental methods to explore the mechanical properties of the microemulsion from the view of atomic size. Unlike other solid materials, a single microemulsion droplet is very difficult to be separated from a microemulsion solution as only investigated target, not even measuring its mechanical properties. Besides, their structure is too tiny to be captured for current experimental methods. Until now, there is no efficient means to evaluate the mechanical properties of a microemulsion droplet.

This work aims to probe the nanomechanics in rupturing microemulsion droplets and to establish the connections between nanoscale mechanical properties of surfactant coated droplets and the molecular structures of microemulsion. Following similar approaches utilizing atomistic modeling and MD simulations[32-34], stable microemulsion droplets were constructed and subjected to rupturing forces. The effects of surfactant structure and the environmental temperature on the droplet rupturing mechanics were scrutinized, which for the first time provided theoretical fundamentals for experimental studies on microemulsion as well as design and processing in practice.

2 MODELS AND METHOD

2.1 Atomistic modeling

In order to realize meaningful microemulsion droplet size for mechanical tests in MD simulations, the transferable potentials for phase equilibria (TraPPE) united-atom parameters[35] were adopted for modeling oil and surfactant molecules, combined with the coarse-grained water, the mW model with many-body force field[36], to build simulation systems[37]. Briefly, the TraPPE united-atom parameters treated non-polar groups, such as the CH_2 group, as one combined atom in the system. The mW water model also considered one water molecule as one combined atom and used a 3-body Stillinger-Weber potential for capturing the appropriate non-bonded interactions among different water molecules[36]. The mW Water model was found to well reproduce the thermodynamic properties of water in many studies[37-39]. Here, dodecane and hexane were modeled as the oil phase. To represent the amphiphile, the linear diblock oligomer surfactants with a varied length of hydrophilic (labeled as L) and hydrophobic (labeled as B) parts were used by modifying the value of force-field parameters between different parts, with details given in Fig. 1, following the similar way with a minimalist model[40]. The bonded potentials, including carbon-carbon single bond, angles, and dihedrals, for the linear oil and surfactant molecules, were borrowed from TraPPE parameters for alkanes[39]. The Lennard-Jones potential (eq (1)) was applied between oil, surfactant and mW water atoms, as details listed in Table 1, similar to the previous studies[35, 41-44]. All the nonbonded interactions were truncated at 9 Å. One can see the energy depth, ϵ of U_{lj} for water atoms (directly borrowed from the mW water model) was two orders of magnitude higher than that for hydrophobic oil atoms (CH_2, directly borrowed from TraPPE parameters[35]), which enabled phase separation between the two. It should be noted that the purpose of the atomic parameters used was for

View Article Online
DOI: 10.1039/D0CP03092A

predicting the qualitative microemulsion droplet rupture mechanics rather than the quantitative value of any specific property.

$$E = 4\epsilon[(\frac{\sigma}{r})^{12} - (\frac{\sigma}{r})^{6}] \quad (1)$$

Four systems were built containing surfactants with different length of hydrophobic and hydrophilic patches (termed L2B4, L2B10, and L4B8) and oil type, as shown in Fig. 1 and Table 2. Other systems consisting of different surfactants can be found in supporting information (Fig. S1). These systems contained the same amount of water (6144), oil (3072) and surfactant (1024) molecules, aiming to form water-in-oil microemulsions. The oil, water, and surfactants were initially distributed orderly in the periodic simulation boxes (209.097 Å × 209.097 Å × 209.097 Å), as shown in Fig. 2 (a). In addition, a large multiphase system consisting of water molecules (32928), L2B10 surfactant molecules (5488) and dodecane oil molecules (16464) was constructed, as shown in Fig. 2 (f)-(j) and Fig. S2. For comparison, we also built up an oil-in-water microemulsion system consisting of water molecules (47928), L2B10 surfactant molecules (5488) and dodecane oil molecules (16464), as shown in Fig. S2. All systems formed stable water-in-oil or oil-in-water microemulsions, which demonstrated the validity of the molecular model and the applied potential.

2.2 Molecular dynamics (MD) simulations

All the MD simulations were performed by using the LAMMPS package[45]. Energy minimization was first carried out with each initial system, employing the steepest descent algorithm. Each system was then equilibrated under the NVT ensemble for 50 ns with a temperature of 400 K by the Nose-Hoover method with a coupling constant of 1 ps with 10 fs time step[46]. The purpose of this high-temperature equilibration was to fully mix the oil, water and surfactant molecules in the systems. Subsequently, the systems were quenched to the NpT ensemble with a temperature of 300 K for another 50 ns. The Parrinello-Rahman barostat was used to keep the system pressure to be 1 bar, with a coupling constant of 1 ps[47]. One stable microemulsion droplet then formed in each system, as shown in Fig. 2 (d), which was then subjected to mechanical testing and rupturing. The simulations before reaching the equilibrium state were run with a constant timestep 10 fs, and during the mechanical deformation and rupture with a constant timestep of 1fs.

To probe the nanoscale de-emulsification mechanics of microemulsion droplets, counter pulling forces were applied onto the water core and the surfactant shell of each microemulsion

droplets, in the same manner as former studies[48, 49]. Briefly, harmonic springs were linked to the center-of-mass of the water core and the surfactant shell, and then displaced at a constant speed. The counter pulling forces were generated and applied onto the droplet owing to the extension of the harmonic springs. In all the droplet rupturing tests, the springs had the same force constant 400 kcal/mol/Å^2 and moving speed 5 nm/ns. Each microemulsion droplet was ruptured at different temperatures in the range of 280~360 K. All simulations end when the core of each microemulsion droplet was separated from the surfactant shell. The rupture work was calculated by integral of pull force on displacement between the water core and the surfactant shell.

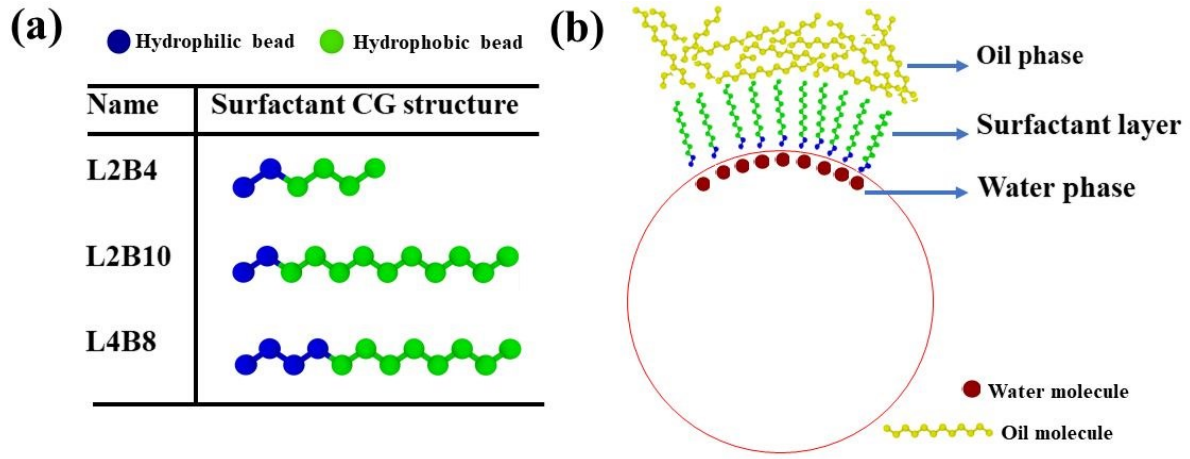

Figure 1. Atomistic models. (a) Janus oligomeric surfactants and their hydrophilic and hydrophobic patches. (b) Schematic of a microemulsion droplet, with a red circle representing the droplet shape. Representative water, surfactant and oil molecules and their locations at the interface of a stable droplet are depicted.

Table 1 The parameters in LJ potential between different atoms.

	ϵ (kcal/mol)	**σ (Å)**
H_2O: H_2O	SW[36]	SW[36]
H_2O: L	0.602	3.558
H_2O: B	0.119	3.558
H_2O: Oil-CH_2	0.119	3.558
L: L	0.602	3.558
L: B	0.091	3.95
L: Oil-CH_2	0.091	3.95
B: B	0.091	3.95

View Article Online
DOI: 10.1039/D0CP03092A

B: Oil-CH_2	0.091	3.95
Oil-CH_2: Oil-CH_2	0.091	3.95

Table 2 Four systems with different surfactants and oil molecules. The surfactants were named by the number of hydrophilic and hydrophobic patches, as depicted in Fig. 1.

System	Surfactant	Oil
A	L2B4	Hexane
B	L2B4	Dodecane
C	L2B10	Dodecane
D	L4B8	Dodecane

3 RESULTS AND DISCUSSION

3.1 Spontaneous formation of stable microemulsion droplets

For evaluating the mechanical properties of microemulsion droplets, four stable microemulsion systems coated with surfactants were prepared with three surfactants and two oil types. Following the defined simulation process of mixing in the NVT ensemble at 400 K and equilibration in the NpT ensemble at 300 K, the final state of all the microemulsion droplets featured a spherical core of water fully coated by surfactants and surrounded by oil molecules, as the representative sequential snapshots are shown in Fig. 2(a-d) and a short video in the supplement (spontaneous-process.MP4). The representative system potential energy profile monitored in preparing the microemulsion droplet was given in Fig. 2(e). Both in the high-temperature mixing simulation and in equilibration, the system potential reached a plateau in a very short time and maintained at that state. The surfactants were packed around the water core, forming an ordered curvature with the hydrophilic patches facing the water. In order to demonstrate the formation process, a larger water-in-oil microemulsion multiphase system was also simulated, as shown in Fig. 2(f-j). The potential energy profile and the packing of surfactants at the oil/water interface agreed with the results predicted in former studies[50].

As shown in Fig. 2, the prepared microemulsion droplets featured the most frequently observed structures, namely water core structure coated by a well-defined surfactant monolayer in the continuous oil phase. The mass ratio between water and oil in the systems was 0.21. The

surfactant shell had long been identified to be critically important to the properties of the microemulsion and was previously found to have an interfacial tension at a threshold of 10^{-3} mN/m[51]. It is known that the interfacial tension of the surfactant layer can compensate for the dispersion entropy of the microemulsion droplets, which contributes to the stability of the microemulsion system[52, 53]. The prepared microemulsion droplets should thus be able to withstand certain pulling force and provide rupturing events for probing the nanoscale de-emulsification.

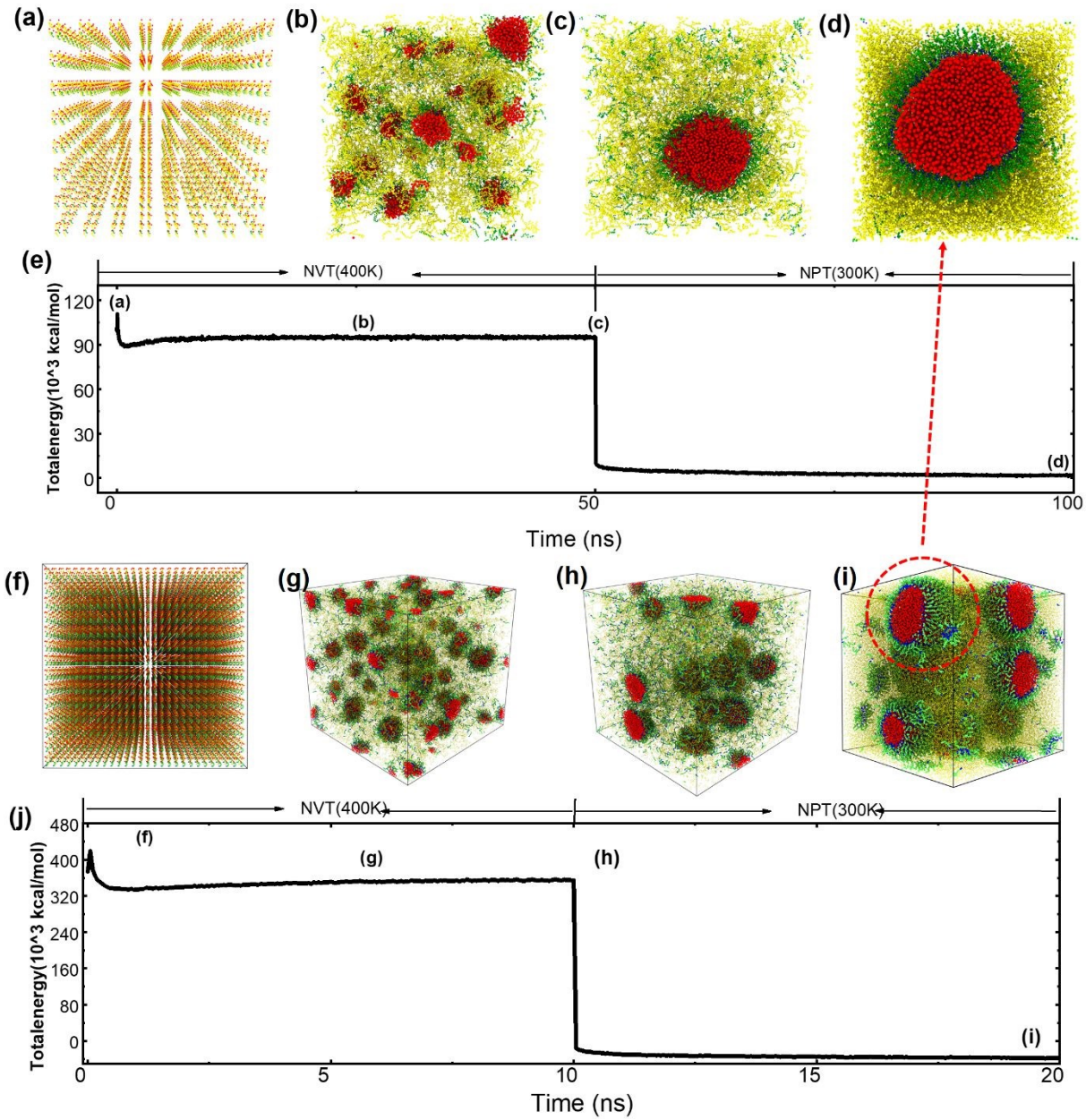

Figure 2. Spontaneous formation of microemulsion droplets, represented by system C. (a) Initial atomistic structure of the systems, with all the components in an orderly arrangement. (b) Disordered and mixing of oil, water and surfactant molecules at 400 K. (c) A complete microemulsion droplet formed at the end of high temperature mixing in the NVT ensemble; (d)

The microemulsion droplet at the end of 50 ns equilibration at 300 K in the NpT ensemble. (e) Total system potential energy. (f-j) the self-emulsifying processes of a multiphase system consisting of water molecules (32928), L2B10 surfactant molecules (5488) and dodecane oil molecules (16464) and the total potential energy.

3.2 The internal structure of the microemulsion droplets

The difference in the surfactants and the oil molecules led to noticeable deviations in the internal structures of the final microemulsion droplets, as shown in Fig. 3. System A and B consisted of the same surfactant but different oil species, namely hexane and dodecane, respectively. The final structure of the two microemulsion droplets showed similar morphologies at the stable state, which suggested that the molecular sizes of hexane and dodecane did not lead to obvious differences in the microemulsion droplet. As shown in Fig. 3 (a-b) and (e-f), the shape of two microemulsion droplets fluctuated in equilibrium, with surfactant molecules randomly adsorbing to and escaping from the oil/water interface. A small fraction of the surfactant molecules could even diffuse into the oil phase as well as into the water core. The result could be attributed to the relatively weak phase preference of the L2B4 molecules (2 hydrophilic and 4 hydrophobic sites in the linear molecule). The stronger hydrophobic or hydrophilic property was needed for the surfactant molecules to firmly coat the internal core of a microemulsion droplet, which was clearly illustrated by comparing the final microemulsion droplets in system B and C, as shown in Fig. 3 (b-c) and (f-g). If the surfactant molecules contained a long hydrophobic patch, 10 hydrophobic atoms in L2B10 instead of 4 in L2B4, the surfactant molecules could not diffuse into the water core, as shown in Fig. 3(c). Thanks to the longer hydrophobic patch in the molecule, the L2B10 surfactant showed more ordered packing at the oil/water interface, and resulted in a more spherical droplet in system C. Because the L2B10 surfactant molecules had the same length of the hydrophilic patch as L2B4 in system A and B, a small fraction of L2B10 were able to escape from the oil/water interface in system C, as shown in Fig. 3(g) and Fig. 4(c). In comparison, system D with L4B8 surfactants was the only system that had a clean oil phase as shown in Fig. 3(h) and Fig. 4(d). Despite the same molecule length of L4B8 surfactants as L2B10, longer hydrophilic patch of L4B8 resulted in the fully locking of all the surfactants at the oil/water interface and an almost perfectly spherical droplet in equilibrium. The packing of the surfactants in system D was the most ordered among the four systems (Fig. 3(d) and Fig. 4(d)). All the results indicated that the surfactant chemistry was the most determining factor of the final state of microemulsion droplets at the nanoscale, consistent with the experimental work[54, 55].

The molecular length and packing orderliness of the surfactants defined the thickness of the microemulsion droplet shell. As shown in Fig. 4(e-h), the shell thicknesses in system A, B, C, and D were 10±2.9, 8±0.6, 15.5±2.1 and 12.4±3.5 Å, respectively (comparison in Fig. S3). The thickness and the packing order of surfactants further influenced the rigidity of the microemulsion droplets, which would induce different de-emulsification behaviour. Besides, the radius of microemulsion droplets in the larger system were in the range of 4-8 nm after equilibration of 2 ns, as shown in Fig. S4. Although the microemulsion system was thermodynamically stable, the size of the microemulsion droplet changed with time due to droplet coalescence. The average radius became larger and larger while the speed of radius increase was getting slower. The speed and the average radius varied from case to case. It was also the reason why different microemulsion systems could keep stable for various time lengths.

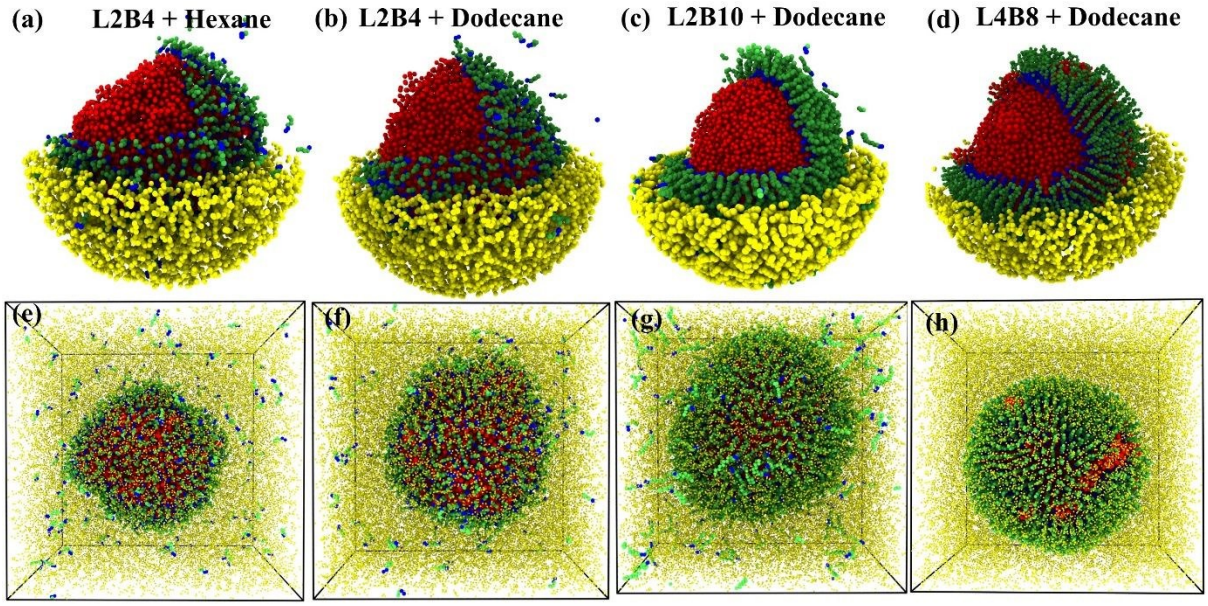

Figure 3. Structures of microemulsion droplets in equilibrium. (a-d) Dissection of the four equilibrated microemulsion droplets with the surfactant and the oil types given on each figure. (e-h) The final system snapshots of the four equilibrated systems in respective order as (a) to (d).

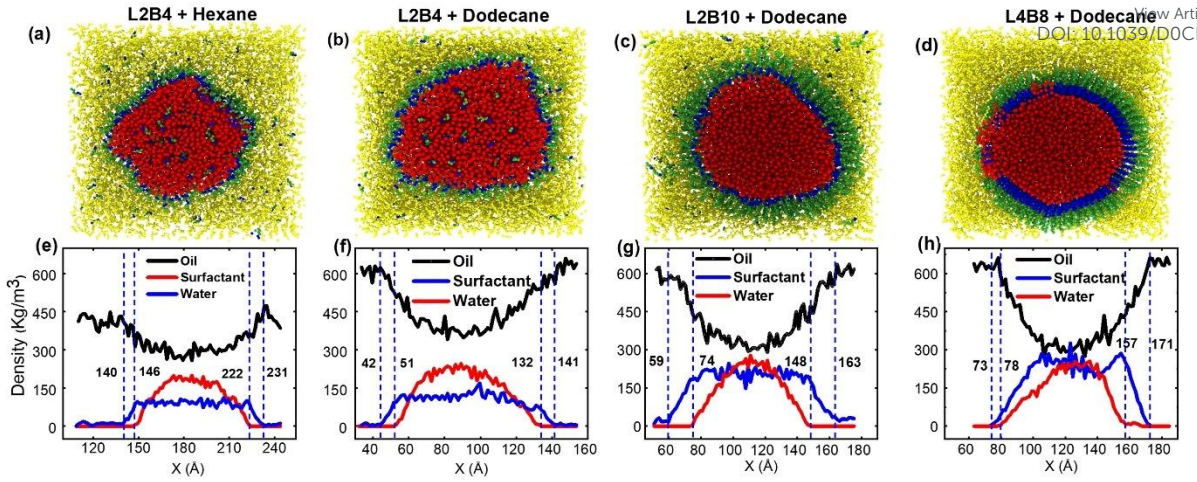

Figure 4. Surfactant shell thickness of the four microemulsion droplets in equilibrium. (a-d) Cross-section view of the four equilibrated droplets, with surfactant and oil type given on top of each figure. (e-h) Representative density distributions of oil, water, and surfactants in representative equilibrated snapshots of the four systems in respective order to (a) to (d). The surfactant shell thickness was quantified as the projected distance on the X-coordinate of the simulation box between the initial point of increasing density of water and surfactant. The blue dash-lines in (e-h) highlight the initial point of increasing density of water and surfactants with coordinates given. The distance between the near-by blue dash-line pair is the surfactant shell thickness.

3.3 Rupture mechanics of microemulsion droplets

3.3.1 Rupturing in nanoscale de-emulsification

The water core and the surfactant shell of each microemulsion droplet were attached to harmonic springs moving on opposite directions, which generated the counterforce on the droplet. Because of the thermodynamic stability of the droplets, a significant force was needed to rupture apart the water core from the surfactant shell, as example system C shown in Fig. 5 and a short video in the supplement (rupture-process.MP4). Force profiles monitored in rupturing all the microemulsion droplets at a temperature below 340 K showed the same pattern of a steady increase to peak values and then a gradual decrease to a low plateau, as shown in Fig. 5. The highest force peak corresponded to the opening of the surfactant shell, while the low force plateau resulted from the friction of the deformed water core with the surfactant shell and the oil phase. For comparison, extra simulations were performed to examine rupture events and rupture forces of the same microemulsion droplets by using different timesteps of 1 and 2 fs. As shown in Fig. S5, the effect of simulation timestep on the rupture behaviour was negligible.

The pulling force monitored before the opening of the surfactant shell showed an almost linear increase, indicating a strengthening behavior of the microemulsion droplet following with a softening process, as shown by the initial part of the force profile and system snapshot 1 in Fig. 5. Releasing the external pulling force before the surfactant shell opening (the peak force value) led to a restoration of the original droplet shape. Such strengthening property was essential to the mechanical stability of microemulsion droplets in experiments, relevant cases of which were drug-carrying droplets transporting through narrow channels.

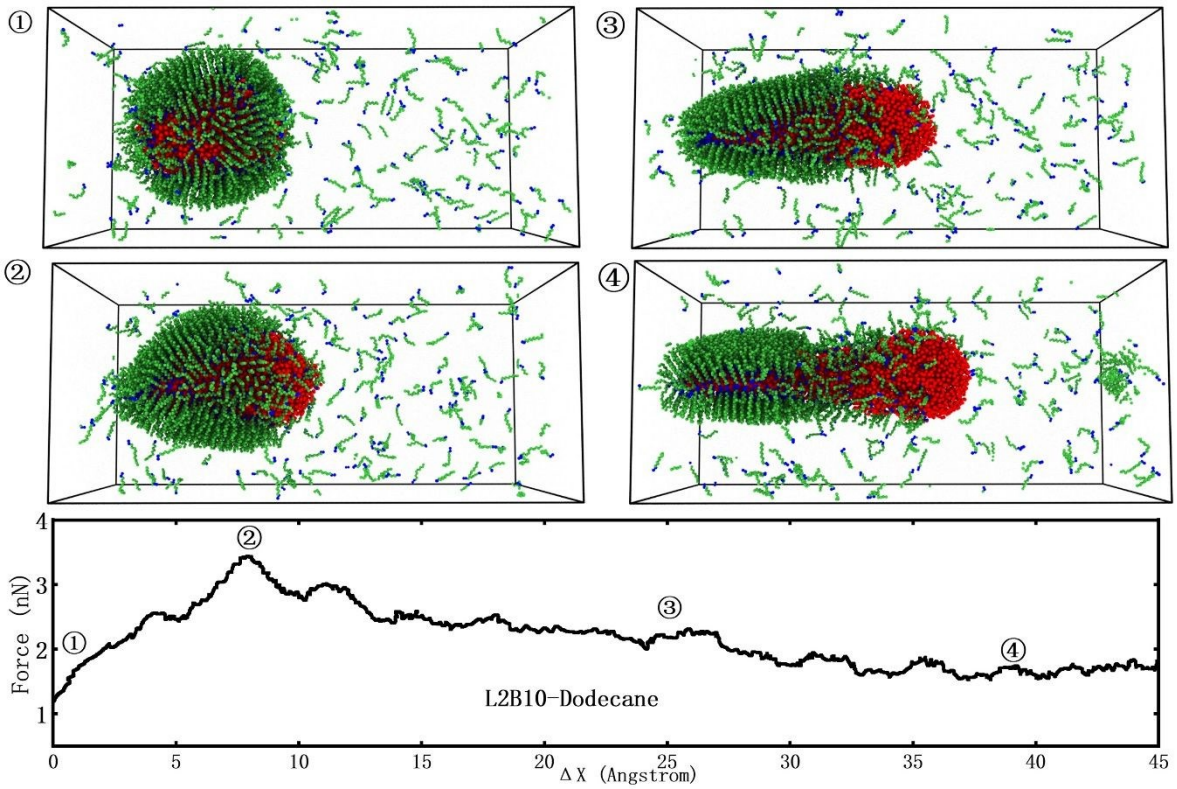

Figure 5. Nanoscale rupturing behaviour of microemulsion droplets represented by system C. Sequential system snapshots, ① - ④, were taken from the one continuous simulation trajectory. The oil molecules were not shown in the figure for a clear view of the microemulsion droplets in the rupturing process. The average force profile monitored in the simulations is given at the bottom, with labels ① - ④ indicating the above corresponding system snapshots. The initial average force is not 0 nN in the figure, which was resulted from the diffusing and shape fluctuation of the droplet. ΔX is the separation distance of the two pulling harmonic spring along with opposite pulling directions.

3.3.2 Temperature effect

The mechanical properties of the microemulsion droplets were greatly affected by temperature owing to the viscosity of the liquid, namely lower temperature resulting in more robust droplets. The four microemulsion droplets were subjected to rupturing force with the same simulation parameters at the varied temperature of 280, 300, 320, 340, and 360 K. The results indicated

that temperature played a major effect on the surfactant shell to influence the mechanical properties of the whole microemulsion droplets. By comparing the force profiles, as shown in Fig. 6, lower temperature resulted in higher peak force and rupture work. High temperature could even diminish the general pattern of the monitored pulling force shown in Fig. 5, especially in system A where the surfactants could easily escape from the oil/water interface (Fig. 3 (a) and (e)). The missing of the force peak at the high temperature indicated that the microemulsion droplet was marginally stable, which coincided with previous experimental observations[56] of high temperature enhancing the thermal motion of the molecules, enlarging the intermolecular distances, and thus weakening the surfactant shell coating on each droplet. The requirement for microemulsion stability differs in the application fields. For instance, robust microemulsion droplets are preferred during transport through channels like in oil production and drug delivery, while weak microemulsions are favorable for subsequent oil separation and drug release[57, 58]. For environments where the temperature range is a non-negligible factor, special attention should be paid to the surfactant composition in the microemulsion system for its stability.

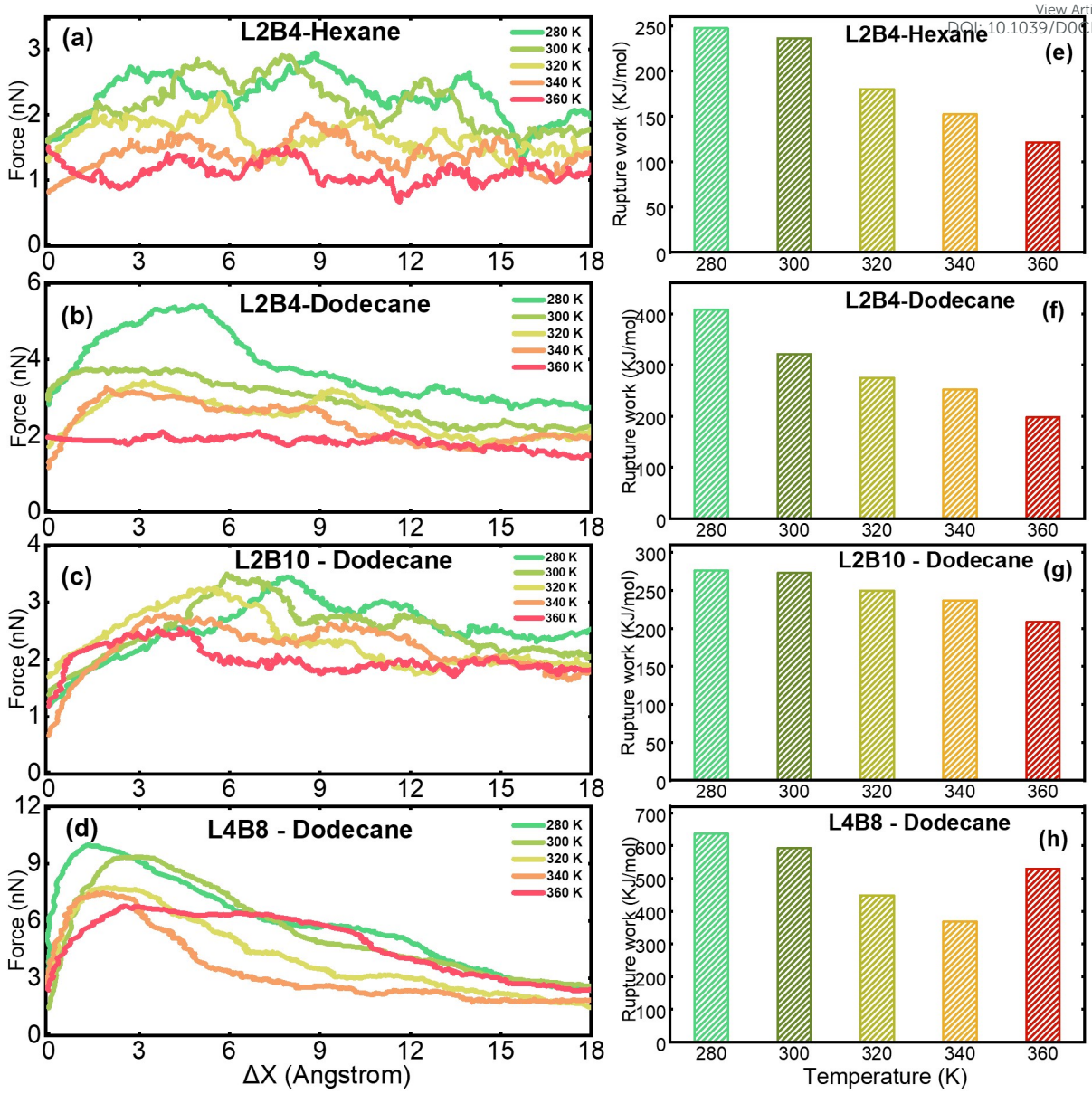

Figure 6. Temperature effect on rupturing the four microemulsion droplets. Force profiles of the four droplet rupturing events are given in (a-d) in the four systems. The surfactant and oil types of each system are given in each figure. The force profiles obtained at different temperatures of 280 K, 300 K, 320 K, 320 K, 340 and 360 K, are labeled by different colors with corresponding legends; the work of fracture of each system at the different temperatures are shown in (e-f).

3.3.3 Surfactant composition effect

The microemulsion droplets in the four systems demonstrated varied mechanical response to the increasing temperature, as shown in Fig. 6. The most robust droplet in system D with a surfactant shell of L4B8 could strongly endure pulling force at the simulation temperature range of 280 ~ 360 K, leading to obvious force peaks compared to its counterparts. As shown

in Fig. 3 (d) and (h), the L4B8 surfactant molecules were highly packed and firmly adsorbed at the oil/water interface. The high orderliness of the surfactants was a result of the optimized amphiphilicity of the molecules and synergically contributed to the mechanical stability of the droplet. Comparing the force profiles of rupturing the four microemulsion droplets at 280 K in Fig. 7, the force peak for opening the L4B8 surfactant shell in system D outperformed its three counterparts. Yet, the highest force peak in system D was observed at the smallest separation distance of two pulling harmonic spring (ΔX) among the four force profiles. As discussed above, the deformed microemulsion droplet could restore its spherical structure and maintain integrity before the opening of the surfactant shell. Highly rigid microemulsion droplets could be difficult to transport through narrow channels if deformation in the droplet shape is required. The other three microemulsion droplets showed much lower surfactant shell opening peak force with larger droplet shape deformation. There is a tendency of higher surfactant packing order leading to higher peak force, more rupture work and smaller droplet deformation in the rupturing simulations.

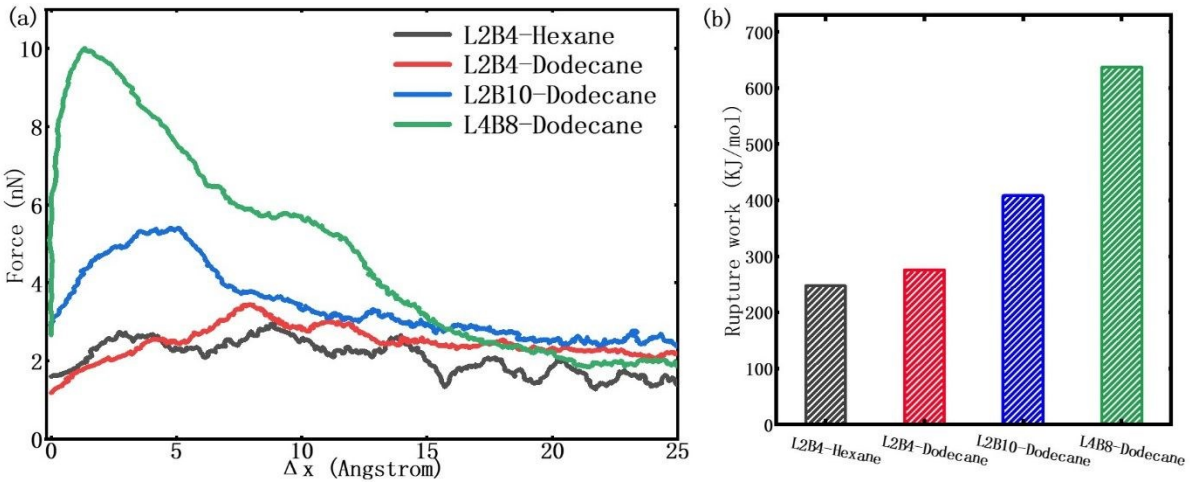

Figure 7. Pulling force profiles with peak values observed in rupturing the four microemulsion droplets in systems A, B, C and D at the temperature of 280 K, shown in (a). the work of fracture of four systems at 280 K are collected into (b). The surfactant and oil types in each system are given as legends.

4 CONCLUSIONS

We have utilized atomistic modeling and molecular dynamics simulation to scrutinize the nanoscale mechanical properties of the microemulsion and resolve the determinants of the droplet stability. The spontaneous emulsification of microemulsion droplets showed that the

structure and arrangement of water and oil interface were dominated by the amphiphilic parts of the linear surfactant molecules. The effects of the chemical composition of the surfactant, the surfactant packing structure and temperature on the droplet rupturing were explored by performing a series of tensile tests. The force peak and the rupture work were obtained to evaluate the robustness of the microemulsions and identify the softening-to-strengthening transition as lowering the temperature. Compared to the previous studies [59-61], this work from the view of MD simulation investigated the morphologies of W/O microemulsion droplets and evaluated their dynamic deformation process. It is the first attempt to scrutinize the mechanical properties of a single microemulsion droplet. Although the loading manner could be different from possible shearing force a microemulsion droplet experienced in experiments, the amplitude of the rupturing force should be proportional to the mechanical stability of the microemulsion droplets. Furthermore, the findings contribute to establishing an atomistic view on microemulsion fluids and provide a general guide to design a stable microemulsion system, such as oil recovery and production, drug delivery, materials fabrication, chemical sensors, and other related fields.

CONFLICTS OF INTEREST

There are no conflicts to declare.

ACKNOWLEDGMENTS

This work is financially supported by the Research Council of Norway (Grant No. 234626) and the Chinese Scholarship Council. The supercomputer CPU hours were provided by the Norwegian Metacenter for Computational science (Project ID: NN9110K and NN9391K).

REFERENCES

1. M. K. Ali, R. M. Moshikur, R. Wakabayashi, M. Moniruzzaman, N. Kamiya and M. Goto, *ACS Sustainable Chemistry & Engineering*, 2020, **8**, 6263-6272.
2. E. Ruckenstein and J. C. Chi, *Journal of the Chemical Society-Faraday Transactions Ii*, 1975, **71**, 1690-1707.
3. A. J. Zarur and J. Y. Ying, *Nature*, 2000, **403**, 65-67.
4. S. Bhattacharya and S. K. Samanta, *Journal of Physical Chemistry Letters*, 2011, **2**, 914-920.
5. Y. Guo, H. Y. Li, Y. H. Yuan, J. Huang, J. Diao and B. Xie, *Journal of Hazardous Materials*, 2020, **386**, 121948.
6. G. Kaur and S. K. Mehta, *International Journal of Pharmaceutics*, 2017, **529**, 134-160.

7. R. Ryan, K. Altria, E. McEvoy, S. Donegan and J. Power, *Electrophoresis*, 2013, **34**, 159-177.
8. A. Fernandez-Pumarega, S. Amezqueta, E. Fuguet and M. Roses, *Analytica Chimica Acta*, 2019, **1078**, 221-230.
9. M. Tagavifar, S. Herath, U. P. Weerasooriya, K. Sepehrnoori and G. Pope, *SPE Journal*, 2018, **23**, 66-83.
10. M. R. Kaiser, Z. Ma, X. Wang, F. Han, T. Gao, X. Fan, J. Z. Wang, H. K. Liu, S. Dou and C. Wang, *ACS Nano*, 2017, **11**, 9048-9056.
11. H. Xie, E. Chen, Y. Ye, S. Xu and T. Guo, *The Journal of Physical Chemistry Letters*, 2020, **11**, 1428-1434.
12. T. P. Hoar and J. H. Schulman, *Nature*, 1943, **152**, 102-103.
13. J. H. Schulman, W. Stoeckenius and L. M. Prince, *The Journal of Physical Chemistry*, 1959, **63**, 1677-1680.
14. H. Mateos, A. Valentini, G. Colafemmina, S. Murgia, E. Robles, A. Brooker and G. Palazzo, *Colloids and Surfaces A: Physicochemical and Engineering Aspects*, 2020, 124801.
15. Y. Cohen, L. Avram and L. Frish, *Angewandte Chemie-International Edition*, 2005, **44**, 520-554.
16. D. P. Acharya and P. G. Hartley, *Current Opinion in Colloid & Interface Science*, 2012, **17**, 274-280.
17. C. D'Andrea, J. Bochterle, A. Toma, C. Huck, F. Neubrech, E. Messina, B. Fazio, O. M. Marago, E. Di Fabrizio, M. Lamy de La Chapelle, P. G. Gucciardi and A. Pucci, *ACS Nano*, 2013, **7**, 3522-3531.
18. A. Paul, K. Meyer, J. P. Ruiken, M. Illner, D. N. Muller, E. Esche, G. Wozny, F. Westad and M. Maiwald, *Measurement Science and Technology*, 2017, **28**, 035502.
19. Y. H. Jin, S. Lohstreter, D. T. Pierce, J. Parisien, M. Wu, C. Hall and J. X. J. Zhao, *Chemistry of Materials*, 2008, **20**, 4411-4419.
20. E. Goldmünz, A. Aserin and N. Garti, *Colloids and Surfaces A: Physicochemical and Engineering Aspects*, 2020, **586**, 124213.
21. M. Rodríguez-Hakim, S. Anand, J. Tajuelo, Z. Yao, A. Kannan and G. G. Fuller, *Journal of Rheology*, 2020, **64**, 799-816.
22. P. Rastogi, N. S. Kaisare and M. G. Basavaraj, *Energy & Fuels*, 2019, **33**, 12227-12235.
23. S. H. Chen and R. Rajagopalan, *Micellar solutions and microemulsions: structure, dynamics, and statistical thermodynamics*, Springer Science & Business Media, 2012.
24. M. Bourrel and R. S. Schechter, *Microemulsions and related systems: formulation, solvency, and physical properties*, Editions Technip, 2010.
25. M. Simon, E. Schneck, L. Noirez, S. Rahn, I. Davidovich, Y. Talmon and M. Gradzielski, *Macromolecules*, 2020.
26. M. L. Klein and W. Shinoda, *Science*, 2008, **321**, 798-800.
27. F. A. Maulvi, A. R. Desai, H. H. Choksi, R. J. Patil, K. M. Ranch, B. A. Vyas and D. O. Shah, *International Journal of Pharmaceutics*, 2017, **524**, 193-204.
28. S. N. Kale and S. L. Deore, *Systematic Reviews in Pharmacy*, 2017, **8**, 39-47.
29. N. Pal, N. Kumar and A. Mandal, *Langmuir*, 2019, **35**, 2655-2667.
30. S. P. Callender, J. A. Mathews, K. Kobernyk and S. D. Wettig, *International Journal of Pharmaceutics*, 2017, **526**, 425-442.
31. R. Nguele, K. Sasaki, Y. Sugai, B. Omondi, H. S. Al-Salim and R. Ueda, *Energy & Fuels*, 2017, **31**, 255-270.
32. N. Arai, K. Yasuoka and X. C. Zeng, *ACS Nano*, 2016, **10**, 8026-8037.
33. S. E. Sherman, Q. Xiao and V. Percec, *Chemical Reviews*, 2017, **117**, 6538-6631.

34. J. Li, J. Wang, Q. Yao, Y. Yan, Z. Li and J. Zhang, *The Journal of Physical Chemistry Letters*, 2020, **11**, 3369-3375.
35. M. G. Martin and J. I. Siepmann, *Journal of Physical Chemistry B*, 1998, **102**, 2569-2577.
36. F. H. Stillinger and T. A. Weber, *Physical review B*, 1985, **31**, 5262-5271.
37. V. Molinero and E. B. Moore, *The Journal of Physical Chemistry B*, 2008, **113**, 4008-4016.
38. C. Vega and J. L. Abascal, *Physical Chemistry Chemical Physics*, 2011, **13**, 19663-19688.
39. W. G. Noid, *The Journal of chemical physics*, 2013, **139**, 090901.
40. N. Arai, K. Yasuoka and X. C. Zeng, *ACS Nano*, 2016, **10**, 8026-8037.
41. L. C. Jacobson, W. Hujo and V. Molinero, *Journal of the American Chemical Society*, 2010, **132**, 11806-11811.
42. B. Raubenolt, G. Gyawali, W. Tang, K. S. Wong and S. W. Rick, *Polymers (Basel)*, 2018, **10**, 475.
43. B. Song and V. Molinero, *The Journal of chemical physics*, 2013, **139**, 054511.
44. G. Gyawali, S. Sternfield, R. Kumar and S. W. Rick, *Journal of Chemical Theory and Computation*, 2017, **13**, 3846-3853.
45. S. Plimpton and B. Hendrickson, ACS Publications, 1995.
46. D. J. Evans and B. L. Holian, *Journal of Chemical Physics*, 1985, **83**, 4069-4074.
47. M. Parrinello and A. Rahman, *Journal of Applied Physics*, 1981, **52**, 7182-7190.
48. S. Xiao, B. H. Skallerud, F. Wang, Z. Zhang and J. He, *Nanoscale*, 2019, **11**, 16262-16269.
49. S. Xiao, Z. Zhang and J. He, *Physical Chemistry Chemical Physics*, 2018, **20**, 24759-24767.
50. J. B. Rosenholm, *Advances in Colloid and Interface Science*, 2020, **276**, 102047.
51. G. Lemahieu, J. Aguilhon, H. Strub, V. Molinier, J. F. Ontiveros and J.-M. Aubry, *RSC Advances*, 2020, **10**, 16377-16389.
52. J. L. Salager, A. M. Forgiarini, L. Marquez, L. Manchego and J. Bullon, *Journal of Surfactants and Detergents*, 2013, **16**, 631-663.
53. X. C. Liu, Y. X. Zhao, Q. X. Li and J. P. Niu, *Colloids and Surfaces a-Physicochemical and Engineering Aspects*, 2016, **494**, 201-208.
54. M. Filippousi, M. Angelakeris, M. Katsikini, E. Paloura, I. Efthimiopoulos, Y. J. Wang, D. Zambouis and G. Van Tendeloo, *Journal of Physical Chemistry C*, 2014, **118**, 16209-16217.
55. P. Golwala, S. Rathod, R. Patil, A. Joshi, D. Ray, V. K. Aswal, P. Bahadur and S. Tiwari, *Colloids and Surfaces B: Biointerfaces*, 2020, **186**, 110736.
56. M. Domschke, M. Kraska, R. Feile and B. Stuhn, *Soft Matter*, 2013, **9**, 11503-11512.
57. C. Torres-Luna, N. Hu, A. Koolivand, X. Fan, Y. Zhu, R. Domszy, J. Yang, A. Yang and N. S. Wang, *Pharmaceutics*, 2019, **11**, 262.
58. B. Hajjar, K.-I. Zier, N. Khalid, S. Azarmi and R. Löbenberg, *Journal of Pharmaceutical Investigation*, 2018, **48**, 351-362.
59. W. X. Shi and H. X. Guo, *The Journal of Physical Chemistry B*, 2010, **114**, 6365-6376.
60. F. Muzaffar, U. Singh and L. Chauhan, *International Journal of Pharmacy and Pharmaceutical Sciences*, 2013, **5**, 39-53.
61. R. Zolfaghari, A. Fakhru'l-Razi, L. C. Abdullah, S. S. E. H. Elnashaie and A. Pendashteh, *Separation and Purification Technology*, 2016, **170**, 377-407.

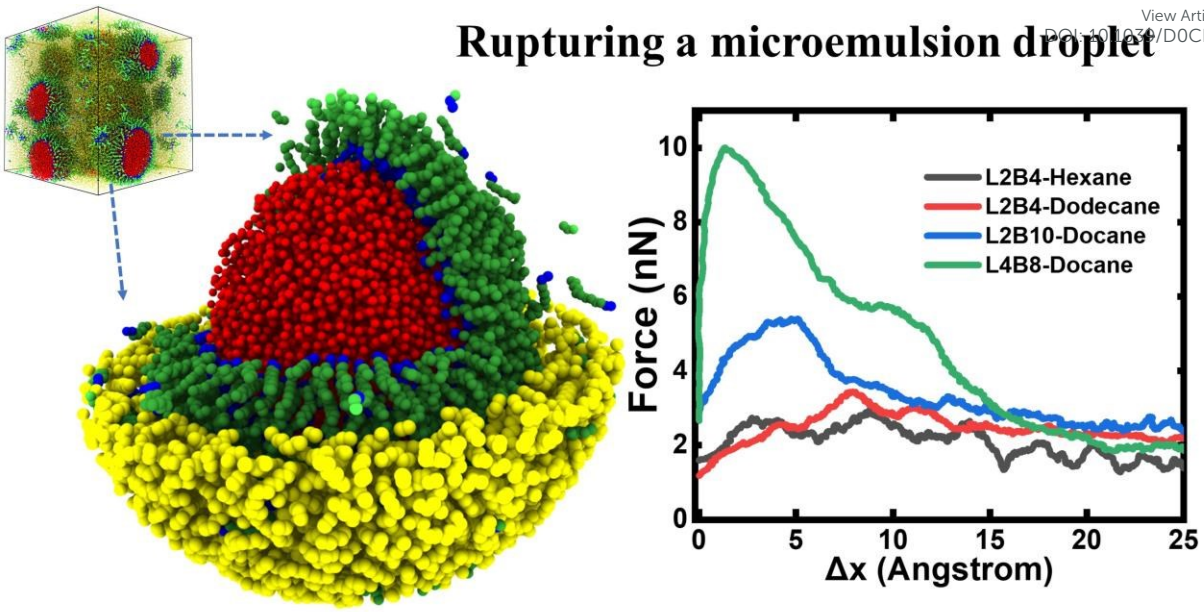

Using counter forces on water core and surfactant shell probed the mechanical stability of microemulsion droplets at different ambient temperatures.